

Structure of Sla1p homology domain 1 and interaction with the NPFxD endocytic internalization motif

Ravi K Mahadev^{1,3}, Santiago M Di Pietro^{2,3},
John M Olson², Hai Lan Piao², Gregory
S Payne^{2,*} and Michael Overduin^{1,*}

¹CR-UK Institute for Cancer Studies, School of Medicine, University of Birmingham, Birmingham, UK and ²Department of Biological Chemistry, David Geffen School of Medicine at UCLA, Los Angeles, CA, USA

Adaptor proteins play important endocytic roles including recognition of internalization signals in transmembrane cargo. Sla1p serves as the adaptor for uptake of transmembrane proteins containing the NPFxD internalization signal, and is essential for normal functioning of the actin cytoskeleton during endocytosis. The Sla1p homology domain 1 (SHD1) within Sla1p is responsible for recognition of the NPFxD signal. This study presents the NMR structure of the NPFxD-bound state of SHD1 and a model for the protein–ligand complex. The $\alpha + \beta$ structure of the protein reveals an SH3-like topology with a solvent-exposed hydrophobic ligand binding site. NMR chemical shift perturbations and effects of structure-based mutations on ligand binding *in vitro* define residues that are key for NPFxD binding. Mutations that abolish ligand recognition *in vitro* also abolish NPFxD-mediated receptor internalization *in vivo*. Thus, SHD1 is a novel functional domain based on SH3-like topology, which employs a unique binding site to recognize the NPFxD endocytic internalization signal. Its distant relationship with the SH3 fold endows this superfamily with a new role in endocytosis.

The EMBO Journal (2007) 26, 1963–1971. doi:10.1038/sj.emboj.7601646; Published online 15 March 2007

Subject Categories: membranes & transport; structural biology

Keywords: endocytosis; NMR; NPFxD; Sla1p homology domain 1

Introduction

Clathrin-mediated endocytosis is a major pathway for internalization of transmembrane receptors. At the molecular level, the process is orchestrated by a network of protein–

*Corresponding authors. GS Payne, Department of Biological Chemistry, David Geffen School of Medicine at UCLA, Los Angeles, CA 90095, USA. Tel.: +1 310 206 3121; Fax: +1 310 206 5272;

E-mail: gpayne@mednet.ucla.edu or M Overduin, CR-UK Institute for Cancer Studies, School of Medicine, University of Birmingham, Birmingham, B15 2TT, UK. Tel.: +44 121 414 3802;

Fax: +44 121 414 4486; E-mail: m.overduin@bham.ac.uk

³These authors contributed equally to this work

Received: 12 October 2006; accepted: 13 February 2007; published online: 15 March 2007

protein and protein–membrane interactions centred on the coat protein clathrin and the multisubunit adaptor complex AP-2 (Traub, 2005). The modular nature of AP-2 facilitates its crucial functions in binding to clathrin, transmembrane cargo, phosphatidylinositol (4,5)-bisphosphate at the plasma membrane, and a host of accessory proteins involved in different stages of endocytosis (Owen *et al*, 2004; Traub, 2005). Other, more specialized adaptors internalize specific cargo proteins but lack the networking ability of AP-2. Recent studies have also pointed to an active role of the actin cytoskeleton in facilitating the process of endocytosis (Perrais and Merrifield, 2005; Kaksonen *et al*, 2006).

Recruitment of transmembrane cargo to endocytic vesicles occurs through adaptor recognition of internalization signals present in cytoplasmic regions of the cargo proteins. In mammalian cells, several types of internalization signals have been extensively studied, including Yxx ϕ and NPxY motifs (where ‘x’ is any residue and ‘ ϕ ’ a bulky hydrophobic residue) and ubiquitin (Hicke and Dunn, 2003; Owen *et al*, 2004; Traub, 2005). Each of these signals is recognized by modular domains within adaptors. Yxx ϕ motifs are bound by a domain within the μ 2 subunit of AP-2 adaptors, NPxY signals by the PTB domain in specialized Dab1/2 and ARH adaptors, and ubiquitin by monoubiquitin-binding domains in specialized adaptors like epsin.

Two types of internalization signals have been defined in yeast: the ubiquitin-based signal recognized by monoubiquitin-binding domains (Hicke and Dunn, 2003) and the NPFxD signal, which is recognized by the Sla1p homology domain 1 (SHD1) found in Sla1p (Tan *et al*, 1996; Howard *et al*, 2002; Piao *et al*, 2007). Sla1p is a specialized adaptor protein which is required for the normal structure and organization of the cortical actin patches that are sites of endocytosis (Holtzman *et al*, 1993; Ayscough *et al*, 1997, 1999; Gourlay *et al*, 2003; Kaksonen *et al*, 2005). It localizes with other endocytic proteins like Sla2p, Pan1p and End3p at actin patches and interacts with a variety of proteins involved in endocytosis and modulation of actin cytoskeleton dynamics (Engqvist-Goldstein and Drubin, 2003; Kaksonen *et al*, 2006). Sla1p consists of three N-terminal SH3 domains followed by SHD1 and SHD2 (unrelated to SHD1), as well as multiple C-terminal LxxQxTG repeats, which are phosphorylated by the Prk1p kinase, thus modulating Sla1p interactions (Ayscough *et al*, 1999; Zeng *et al*, 2001).

SHD1 is a protein interaction domain in Sla1p that specifically recognizes NPFxD-type internalization signals found in the cytoplasmic domains of transmembrane proteins like the a-factor receptor Ste3p, the Golgi-resident furin-like protease Kex2p and the cell wall stress sensor Wsc1p (Tan *et al*, 1996; Howard *et al*, 2002; Piao *et al*, 2007). This interaction leads to endocytosis in an SHD1- and NPFxD-dependent manner. All four amino-acid residues defining the NPFxD signal have been shown to be important for efficient endocytosis (Tan *et al*, 1996; Howard *et al*, 2002).

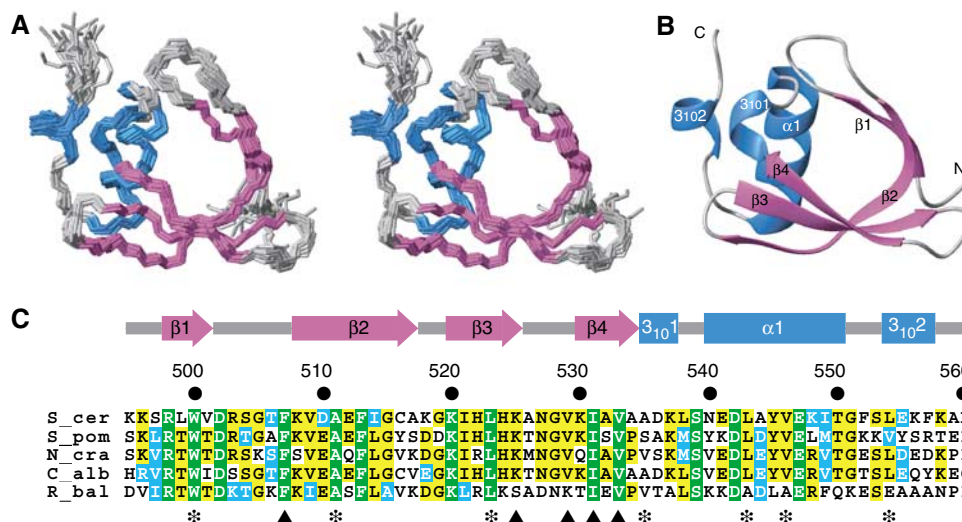


Figure 1 Solution structure of SHD1 and sequence alignment. (A) Stereoview of the NMR ensemble of 20 best structures for SHD1. Residues Arg498–Val501 in β1, Lys508–Ala517 in β2, Lys520–Lys525 in β3, Lys530–Thr550 from β4 to α1 and Leu554–Phe557 in 3₁₀2 were used for the superposition. (B) Ribbon representation of SHD1. The secondary structure elements and termini are labelled, with β-strands coloured magenta; helices, blue; and loops and termini, gray. Panels A and B were generated using MOLMOL (Koradi *et al*, 1996). (C) Sequence alignment of representative fungal and bacterial SHD1 sequences. Fully conserved residues are highlighted in green, partially conserved residues in yellow and substitutions with similar residues in cyan. Conserved residues in the hydrophobic core and the ligand-binding site are marked with (*) and (▲), respectively, at the bottom of the alignment. SHD1-related sequences were identified using PSI-BLAST (Altschul *et al*, 1997). The alignment was created using CLUSTALW (Thompson *et al*, 1994) and BOXSHADE tools in the SDSC Workbench (Subramaniam, 1998). Sequences used are *Saccharomyces cerevisiae*, *Schizosaccharomyces pombe*, *Neurospora crassa*, *Candida albicans* and *Rhodopirellula baltica*. The last, [R_bal] bacterial sequence contains the least well-conserved SHD1, and the host protein lacks the SH3 domains usually found in Sla1p homologues, suggesting functional divergence. Close homologues of SHD1 are not evident in higher eukaryotes.

To better understand the molecular recognition of NPFxD by SHD1, the three-dimensional (3D) structure of Sla1p SHD1 in the presence of an NPFSD ligand sequence has been determined. Results from NMR and structure-based mutagenesis map specificity determinants for the SHD1:NPFxD interaction, allowing a model for the SHD1–NPFSD complex to be derived. The model is supported by inhibitory effects of mutating key interaction residues on ligand binding *in vitro* and receptor internalization *in vivo*.

Results and discussion

Solution structure of SHD1

The structure of SHD1 from Sla1p was determined in the presence of Kex2p peptide ligand using ¹³C, ¹⁵N-resolved NMR methods (Figure 1A and B). The fold consists of a highly twisted β-sheet followed by a C-terminal helical motif. The four antiparallel β-strands form an open barrel capped by a long α-helix bordered by two short 3₁₀ helices. The ensemble of 20 structures has a root mean square deviation (RMSD) of 0.34 ± 0.06 Å for backbone atoms and 0.77 ± 0.06 Å for all heavy atoms, calculated from the mean structure. Structural statistics data for SHD1 are shown in Table I. A solvent-accessible hydrophobic pocket is evident on the open face of the barrel opposite the helical cluster, and consists of residues Phe507, Val509 in β2, Lys525 in β3, Val529, and β4 residues Ile531 and Val533. The hydrophobic core of the protein is composed of Trp500 in β1, Ala511 in β2, Leu523 in β3, Ala535 in the first 3₁₀ helix, Leu538, α-helical residues Leu543 and Val546, and Leu554 in the second 3₁₀ helix. The residues in the pocket and core are highly conserved (Figure 1C), indicating a common fold and function of

Table I NMR restraints and structural statistics for SHD1

Distance restraints	
Intraresidue ($i-j=0$)	222
Sequential ($ i-j =1$)	264
Medium range ($2 \leq i-j \leq 4$)	169
Long range ($ i-j \geq 5$)	274
Hydrogen bonds	52
Total	981
Dihedral angle restraints from TALOS	
Phi (ϕ), Psi (ψ)	39,39
RMSD of atomic coordinates (Å)	
Backbone heavy atoms	0.34 ± 0.06
All heavy atoms	0.77 ± 0.06
RMSD from experimental restraints	
Distances (Å)	0.041 ± 0.002
Dihedral angles (deg)	0.453 ± 0.108
Violations	
Distances > 0.5 Å and dihedral angles > 5°	Nil
Ramachandran plot analysis, (% residues)	
Most favorable region	88.9
Additional allowed regions	10.1
Generously allowed regions	0.5
Disallowed regions	0.6

SHD1 domains, which are found in a variety of fungi and several bacteria.

Model of the SHD1–NPFxD complex

The interactions of the Kex2p and Ste3p peptide ligands were evident from extensive chemical shift perturbations (CSP) seen in the ¹⁵N HSQC spectra of SHD1 (Figure 2A). The Kex2p peptide, NENPFSDPIK, bound to SHD1 in the intermediate exchange regime whereas the Ste3p peptide, SRNPFSTDSE, bound more weakly, exhibiting fast exchange on the NMR

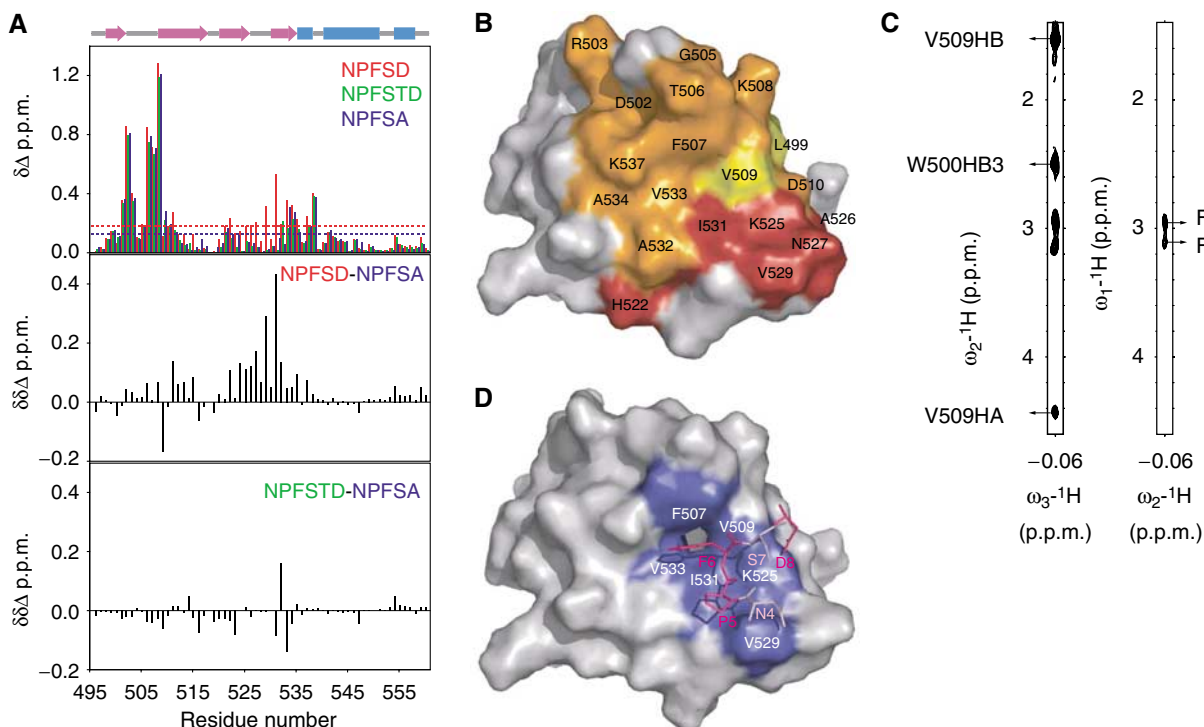


Figure 2 Ligand binding to SHD1. **(A)** The top panel shows residue-wise CSP in SHD1 upon addition of saturating amounts of Kex2p, Ste3p and NPFSA peptides, calculated as $\sqrt{\{(\delta\text{H})^2 + (\delta\text{N}/5)^2\}}$. The average CSPs for Kex2p (---) and NPFSA (---) binding are marked. The middle and the bottom panels show the difference in CSPs of the NPFSA peptide from those of the Kex2p and Ste3p peptides, respectively. The secondary structures along the sequence are shown on the top. **(B)** Surface map of perturbed residues in SHD1 upon Kex2p and Ste3p binding. Residues perturbed upon Kex2p binding are in red, those perturbed upon Ste3p binding are in yellow and residues perturbed in response to both the peptides are in orange. **(C)** Strips from 3D $^{15}\text{N}/^{13}\text{C}$ -edited NOESY and 2D ^{13}C -edited, $^{15}\text{N}/^{13}\text{C}$ -filtered NOESY to show intermolecular NOEs for the Val509 methyl side-chain residue. **(D)** Model for the SHD1-NPFSD complex. SHD1 is shown in surface representation. The core NPFSD residues are shown in stick representation. Residues in SHD1 that show intermolecular NOEs and are known to be important based on mutagenesis studies are shown in deep blue. The Pro5, Phe6 and Asp8 residues are experimentally restrained and are shown in dark magenta, whereas residues Asn4 and Ser7, which are only restrained by HADDOCK, are shown in light magenta. Panels B and D were generated using PYMOL (DeLano, 2002).

timescale. Compared to the Ste3p peptide, the Kex2p peptide induced unique and more extensive perturbations in a SHD1 surface patch involving Lys525, Ala526, Asn527, Val529 and Ile531 (Figure 2B), implicating these residues as key specificity determinants for the NPFxD motif from Kex2p.

The Kex2p NPFxD motif was selected for characterization of the SHD1 complex, as it bound to SHD1 with a slower apparent off-rate compared to the Ste3p NPFxD motif. Intermolecular nuclear Overhauser effect (NOE) contacts were observed involving Val509, Val529, Ile531, Val533 and Leu538 in the $^{15}\text{N}/^{13}\text{C}$ -edited NOE and filtered NOE spectra (Figure 2C). Based on their assignments in the free Kex2p peptide, 17 unambiguous intermolecular NOEs were attributed to Kex2p residues Pro5 (six NOEs) and Phe6 (11) and SHD1 residues I531 (six NOEs), V509 (6), V529 (3), V533 (1) and L538 (1). Assignments of the remaining peptide residues in their bound states were complicated by conformational exchange and line broadening. Consequently, NOEs to the Asn4 and Asp8 ligand residues could not be unambiguously assigned, whereas other peptide residues did not show any detectable NOEs.

NMR experiments with a mutant 'NPFSA' Kex2p peptide in which Ala was substituted for the conserved Asp suggested an Asp interaction element in the H524-A532 sequence (Figure 2A, see below), and mutagenesis of SHD1 implicated K525 in recognition of the Asp in NPFSD (Figure 3B, see below). To calculate the model of the SHD1-NPFxD complex,

therefore a distance restraint of 3 Å between the ends of the K525 (SHD1) and Asp8 (NPFxD) side chains was also included.

A model for the SHD1-NPFxD complex was calculated with the programme HADDOCK (Dominguez *et al*, 2003) using restraints based on 17 intermolecular NOEs as well as the CSPs in the ^{15}N HSQC experiment. The ensemble of the 20 energetically most favourable structures yielded RMSDs of 0.54 ± 0.24 and 0.87 ± 0.31 Å for backbone and heavy atoms, respectively, spanning SHD1 Ser497-Lys558 and Kex2p Asn4-Asp8 sequences.

The model of the complex is shown in Figure 2D, and depicts the Pro5 and Phe6 residues of the ligand in the centre of the hydrophobic binding site on the SHD1 surface. The Pro5 residue was positioned close to K525, Val529 and Ile531 of SHD1, whereas Phe6 packed against F507, V509, K525, I531 and V533. The Asp8 residue was oriented near K525 in SHD1 and across from Asn4, whereas the remainder of the peptide, being unconstrained, was disordered.

Role of binding site residues in complex formation

The contribution of SHD1 residues in and around the hydrophobic binding pocket to NPFSD recognition was investigated using surface plasmon resonance (SPR). Binding of wild-type and mutant SHD1 proteins to an NPFSD peptide was measured. SHD1 binding to NPFSD was concentration-dependent and saturable (Figure 3A), with a K_d of approximately 5 μM

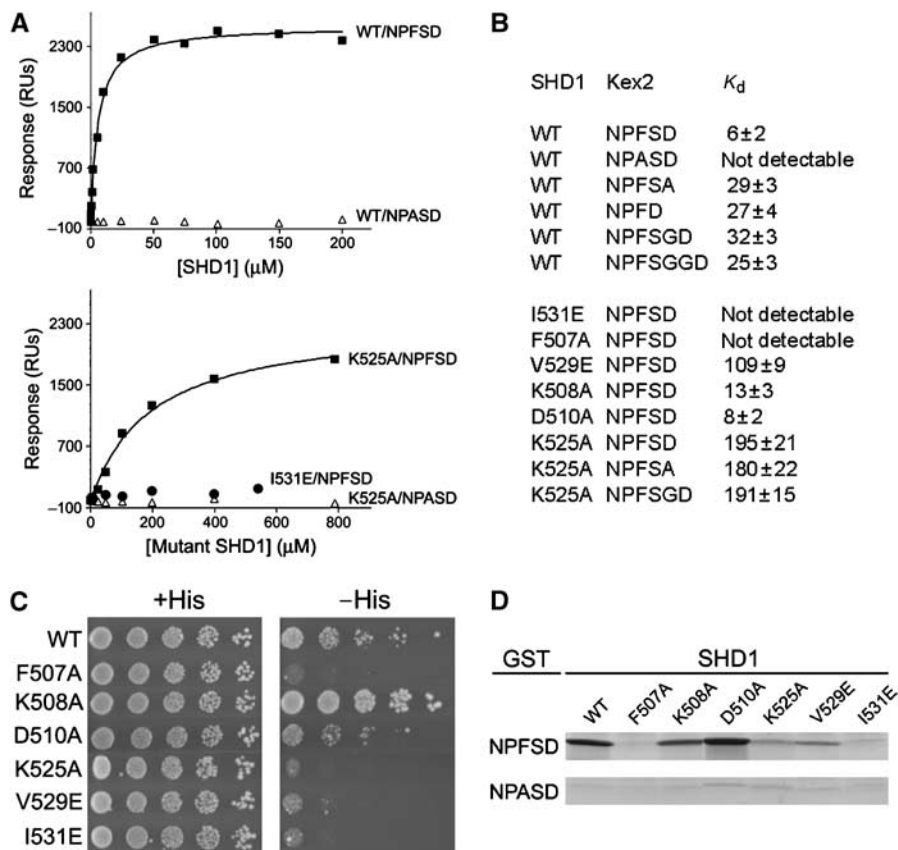


Figure 3 Mutagenesis studies on binding site residues. (A) SHD1 hydrophobic pocket residues are important for NPFSD binding. (Upper panel) Binding of SHD1 to an NPFSD peptide (■) or an NPASD peptide (Δ) measured by SPR. (Lower panel) Binding of SHD1–K525A to an NPFSD peptide (■) or an NPASD peptide (Δ) and SHD1–I531E to an NPFSD peptide (●). (B) The affinities of NPFSD and variants binding to wild-type and mutant SHD1, as measured by SPR, are listed. (C) NPFSD interaction with wild-type and mutant SHD1 assayed by yeast two-hybrid assays. Wild-type SHD1 and mutant versions were fused to the Gal4 activation domain (GAD) and tested for interaction with three repeats of the NPFSD signal linked to the Gal4 DNA-binding domain (GBD). Serial dilutions of cells were grown at 30°C on synthetic media containing (+ His) or lacking (– His) histidine. (D) NPFSD binding to wild-type and mutant SHD1 assayed by GST fusion protein affinity. Purified wild-type SHD1 and the indicated mutants were tested for interactions with GST fused to triple repeats of active (NPFSD) or inactive (NPASD) forms of the Kex2p-derived signal. Eluted proteins were subjected to SDS–PAGE and visualized by Coomassie blue staining.

(Figure 3B). As expected, binding to an endocytically inactive NPASD mutant peptide was negligible (Figure 3A). Mutations F507A and I531E completely abolished the interaction whereas mutations K525A and V529E had strong effects (Figure 3A and B), emphasizing the crucial role of these residues in the binding pocket. In contrast, K508A had a weak effect and D510A a negligible effect on binding. Similar effects of mutations on binding were observed in yeast two-hybrid and GST-fusion affinity interaction assays (Figure 3C and D). These mutant SHD1 proteins were folded as assessed by circular dichroism spectroscopy, whereas mutations involving residue V509, V533 or L538 yielded insoluble or poorly folded domains following cleavage from GST.

Specificity determinants for Asp in signal binding

Previous work demonstrated that mutation of the Asp in NPFSD reduced but did not eliminate endocytosis mediated by the Kex2p signal, suggesting an important but not essential role for this residue in binding SHD1 (Tan *et al*, 1996). Additionally, weaker binding of SHD1 to the Ste3p NPFSTD peptide compared to the Kex2p peptide detected by NMR raised the possibility that spacing between the ligand Phe and Asp residues in the signal plays a role in binding efficiency.

To further address the role of the Asp residue and its spacing from the NPF motif in binding, SPR was used to measure binding of NPFSA, NPFD, NPFSD, NPFSGD and NPFSGGD peptides to SHD1. As shown in Figure 3B, substitution of Ala for Asp in the Kex2p ligand, or any change in the Asp position reduced affinity by a factor of 5. Thus, both the presence and spacing of the Asp play significant although not essential roles in NPFxD signal recognition by SHD1.

To identify determinants of Asp recognition, SHD1's site of interaction with the NPFSA mutant peptide was mapped by NMR. CSPs observed in the ^{15}N HSQC spectra due to NPFSA addition were compared to those caused by the Kex2p and Ste3p peptides. Interaction of the mutant peptide resembled the binding mode of the weaker Ste3p ligand, inducing smaller perturbations in the H524–A532 region involved in wild-type Kex2p peptide binding (Figure 2A and B). This result suggested that this region harbours a specificity element for the Asp residue in the NPFxD motif. An attractive candidate is K525, which undergoes CSPs upon NPFSD binding and is important for signal binding. This interaction was further explored by measuring binding of NPFSD, NPFSGD and NPFSA peptides to the K525A mutant of SHD1. As shown in Figure 3B, the SHD1 mutant did not discriminate between the peptides, exhibiting 30-fold reductions

in affinity compared to the affinity of wild-type SHD1 for NPFSD. These data strongly implicate K525 in recognition of the Asp in NPFSD, for example, through a stabilizing electrostatic interaction. However, the affinity of the K525A SHD1 mutant for NPFSD is significantly lower than that of wild-type SHD1 for the reciprocally compromised NPFSA peptide, suggesting that K525 contributes to NPFSD binding through additional interactions.

SHD1 binding site residues are critical for receptor endocytosis

To test the role of the hydrophobic binding pocket of SHD1 in NPFxD-dependent endocytosis *in vivo*, SHD1 mutations were introduced into the endogenous *SLA1*. Each mutant was expressed at normal levels as assessed by immunoblotting (Figure 4A). Mutant effects on endocytosis were assessed using strains expressing a chimeric plasma membrane receptor in which the NPFSD signal from Kex2p replaced the cytoplasmic C-terminal domain of the α -factor mating pheromone receptor, Ste2p (Howard *et al*, 2002). This receptor (Ste2p Δ 318-NPFSD) exhibits normal pheromone binding but lacks the native ubiquitin-dependent targeting signals in the Ste2p cytoplasmic tail, thereby conferring complete dependence on the appended NPFSD signal for pheromone endocytosis. The internalization of Ste2p Δ 318-NPFSD in wild-type and SHD1 mutant strains was monitored by measuring uptake of radiolabeled α -factor. As shown in Figure 4B, the *SLA1* I531E mutation eliminated α -factor internalization whereas D510A had no effect compared to wild type. This result is consistent with the *in vitro* binding and NMR data that identify I531 as a critical residue for the interaction and position D510 close to, but outside, the binding pocket. Uptake of α -factor was completely abolished in K525A mutant cells and nearly absent in V529E mutant cells (Figure 4C). Considering the effects of these mutants on the affinity of SHD1 for NPFSD *in vitro*, the appearance of limited endocytosis in the V529E mutant (K_d 109 μ M; Figure 3B) suggests that an affinity of about 100 μ M is the minimum required for an effective interaction with the Ste2p Δ 318-NPFSD receptor *in vivo*. Also in agreement with *in vitro* binding results, F507A mutant cells were completely defective in endocytosis and K508A mutant cells were only marginally defective (Figure 4D). Taken together, our results indicate striking parallels between effects of structure-based mutations on endocytosis *in vivo* and signal binding *in vitro*, providing strong support for the physiological significance of the NMR-derived structure.

SHD1 binding site residues are important for endocytosis-dependent function of a cell wall stress sensor

It has been recently reported that the major cell wall stress sensor Wsc1p relies on an NPFxD signal and SHD1 for constitutive endocytosis (Piao *et al*, 2007). NPFxD-dependent internalization and endocytic recycling to the plasma membrane are necessary to maintain polarized distribution of Wsc1p to sites of new cell surface growth. Mutation of the Wsc1p NPFxD signal or deletion of SHD1 from *SLA1* prevents Wsc1p endocytosis and leads to uniform accumulation along the cell surface. Depolarization of Wsc1p due to defects in endocytosis compromises the ability of the sensor to respond to cell wall stress imposed by the cell wall synthesis inhibitor

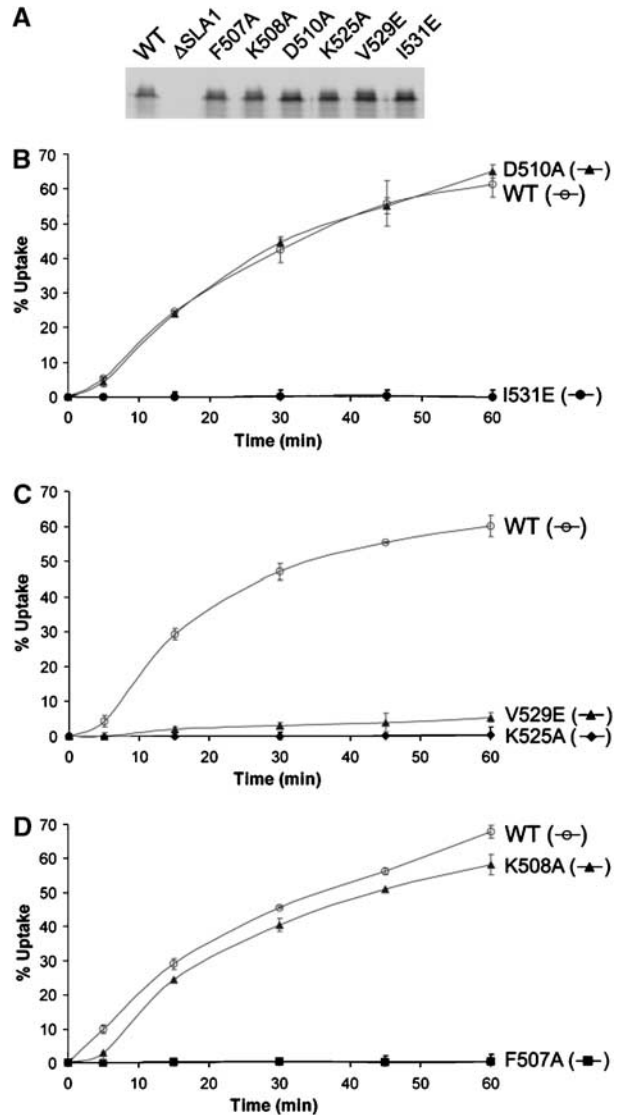


Figure 4 NPFSD-mediated endocytosis requires SHD1 signal binding pocket residues. (A) Total yeast cell extracts from GPY1805, a *sla1* Δ strain (GPY2448) (Howard *et al*, 2002) and the *Sla1p* SHD1 mutant strains were analyzed by SDS-PAGE and immunoblotting with *Sla1p* antibodies. (B–D) Uptake of prebound, radiolabeled α -factor was measured in GPY1805 (*Sla1p* wild-type strain, WT) and the indicated *Sla1p* mutant strains expressing Ste2p Δ 318-NPFSD at 30°C. Error bars represent the s.d. in two separate samples.

casprofungin (Piao *et al*, 2007). Thus, growth on medium containing casprofungin provides a facile and sensitive measure of NPFxD-mediated internalization of Wsc1p. Accordingly, to monitor the effects of the SHD1 binding site mutations on internalization of a native plasma membrane protein, SHD1 mutants were tested for growth in the presence of casprofungin (Figure 5A). Mutations in I531, K525, V529 and F507 caused increased sensitivity, whereas mutations in K508 and D510 did not.

Wsc1p localization was directly examined in a subset of mutant strains expressing a functional Wsc1p-GFP fusion. In parallel to the casprofungin sensitivity results, mutation of I531 and K525, but not D510, caused cell surface depolarization of Wsc1p-GFP at 24°C, indicative of defective endocytosis (Figure 5B). Effects of mutations on Wsc1p-GFP

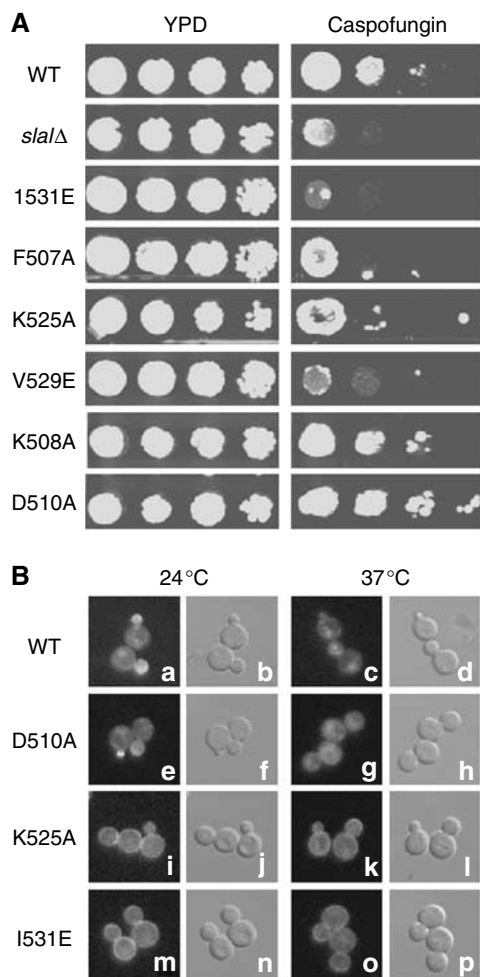


Figure 5 SHD1 binding pocket residues are required for Wsc1p-mediated cell wall stress response and Wsc1p endocytosis. (A) Wild-type (WT; GPY1805), *sla1Δ* (GPY2448) and SHD1 mutant cells were grown in YPD media and five-fold serial dilutions were spotted onto YPD or YPD containing 350 ng/ml caspofungin. (B) Wild-type (WT; GPY3527) and SHD1 mutants were grown to early log phase and then treated with or without heat shock at 37°C for 35 min. Cells were visualized by epifluorescence (left panel in each pair) and differential interference contrast (DIC) microscopy (right panel in each pair).

internalization were more clearly evident after cells were shifted to 37°C, a treatment that stimulates sorting of internalized Wsc1p-GFP to the vacuole in wild-type cells (Piao *et al*, 2007). In contrast to wild-type and D510A cells, where Wsc1p-GFP was internalized and delivered to the vacuole, the protein remained uniformly distributed at the surface of I531E and K525A cells (Figure 5B). These results offer further support for the SHD1 structural model and indicate that endocytosis mediated by the NPFxD binding site plays an important physiological role in the yeast cell wall stress response pathway.

SHD1 is related to domains based on the SH3 type fold

Comparison of the SHD1 structure to known protein structures using DALI (Holm and Sander, 1993) identifies close structural matches to protein domains having the SH3 barrel fold, despite low sequence similarity. The closest structural neighbour is the Sm-like domain in the RNA-binding translational regulator protein Hfq (Schumacher *et al*, 2002)

(Figure 6A). The most similar SH3 domain that binds to polyproline type II helix (PPII) motifs is the one from p40^{phox} (Massenet *et al*, 2005) (Figure 6B). When the residues involved in ligand binding are compared (Figures 6C–E), the unique binding site in SHD1 is evident. In contrast to the binding site formed by residues lining β2 and β4 of SHD1, the Hfq RNA-binding site is formed by residues in the N-terminal α-helix, the loop connecting β2 and β3 and residues in the loop following β4 (close to Ala535 and Asp536 in SHD1). However, some residues lining β1 and β4 form part of the oligomerization interface (Figure 6C). Comparison to p40^{phox} SH3 domain reveals that two residues, Pro 220 and Phe 223, occur at positions adjacent to Val533 (in β4) and Leu538, respectively, in SHD1. However, the p40^{phox} SH3 PPII binding site also comprises crucial residues in the RT loop (Figure 6E), which is missing entirely from SHD1. Thus, SHD1 is a novel functional domain based on the SH3-like polypeptide fold that is fundamentally distinguished by its unique binding pocket, the inclusion of C-terminal helices and the absence of an RT loop.

Sla1p as an endocytic adaptor

Sla1p is required for the normal functioning of the actin cytoskeleton during endocytosis (Engqvist-Goldstein and Drubin, 2003; Kaksonen *et al*, 2006). Participation in cargo binding by SHD1 recognition of NPFxD motifs makes Sla1p the only adaptor known to link endocytic cargo and actin dynamics in either yeast or mammals. The lack of obvious SHD1 motifs in higher eukaryotes suggests that its role may have been taken on by other modules, such as NPF-binding EH domains (de Beer *et al*, 2000) or FxNPFxY-binding PTB domains (Stolt *et al*, 2003). Although mammalian homologues of Sla1p are not obvious by sequence comparisons, the Sla1p/Pan1p/End3p complex (which contains three SH3, SHD1, SHD2 and five EH domains) in yeast is considered functionally equivalent to the Intersectin/Eps15 complex (five SH3 and five EH domains) in mammals (Howard *et al*, 2002; Kaksonen *et al*, 2006). However, neither Intersectin nor Eps15 is known to bind directly to internalization motifs in endocytic cargo proteins. The SH3-like domain structure of SHD1 furthers the similarity of the Sla1p and Intersectin complexes in terms of SH3 composition, and suggests that SHD1 is a divergent SH3 domain that has acquired the ability to recognize an NPFxD type receptor internalization signal. Alternatively, Sla1p may be analogous to CIN85, an endocytic scaffold with a domain organization (three N-terminal SH3 domains) and interaction profile similar to Sla1p (Stamenova *et al*, 2004), although CIN85 also lacks SHD1/2-like regions.

In summary, this study presents the solution structure of the ligand-bound state of SHD1, a recently discovered protein interaction domain for the recognition of NPFxD type internalization motifs present in transmembrane endocytic cargo proteins. The structure is composed of an SH3-like polypeptide fold, making it the first example of an SH3-like family member with an ability to bind an endocytic internalization signal. The structure consists of a highly twisted β-sheet followed by a C-terminal helical motif and contains a unique solvent-exposed hydrophobic binding site. A structural model of the SHD1–NPFxD interaction indicates that SHD1 uses this site to bind the NPFxD internalization signal.

Extensive structure-based mutagenesis studies confirm the role of conserved hydrophobic binding site residues in signal

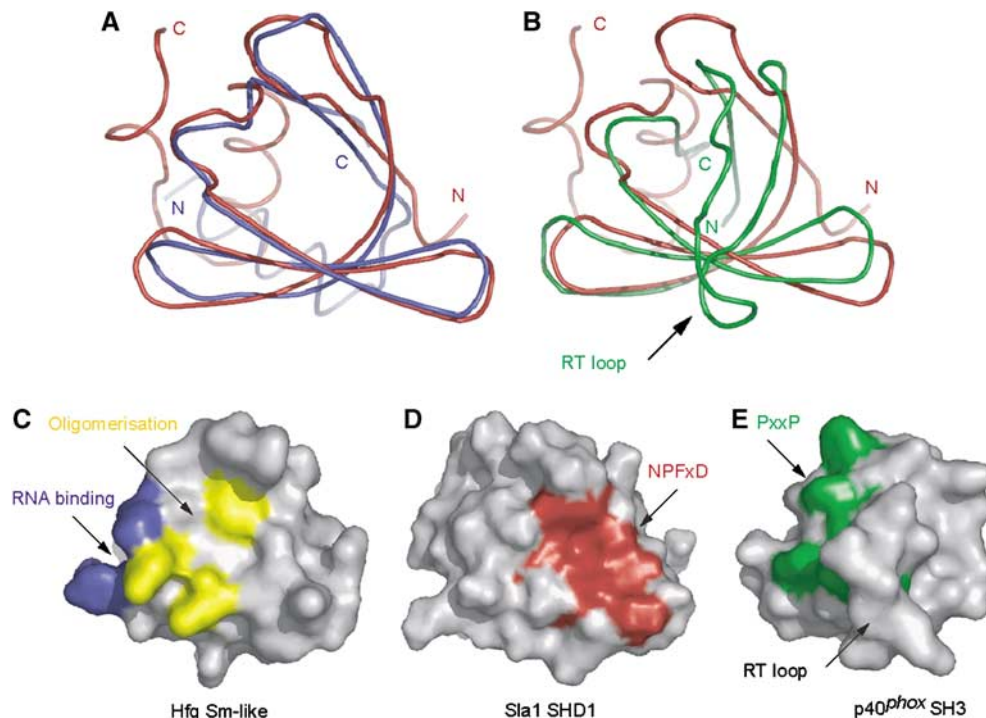


Figure 6 Representative structural neighbours of SHD1. (A, B) Sm-like domain from translational regulator Hfq (PDB ID 1KQ1) with a Z-score of 4.3 and SH3 domain from p40^{phox} (PDB ID 1W6X) with a Z-score of 2.1. C α -based superposition gives an RMSD of 2.7 Å for Sm-like domain over 45 residues (with 13% sequence identity) and 2.8 Å for the SH3 domain over 40 residues (5% sequence identity). SHD1 is shown in red, the Sm-like domain in blue and the SH3 domain in green. (C–E) Surface representations Hfq, SHD1 and p40^{phox}-SH3 to highlight the difference in binding pockets in the three proteins. The residues, on the similar surfaces, that form the binding site are highlighted in blue, red and green, respectively. In the case of Hfq, residues involved in oligomerization are shown in yellow. All figures were generated using PYMOL (DeLano, 2002).

recognition. They further establish that, although the interaction is largely hydrophobic, optimal binding depends on the Asp residue and the spacing between NPF and D. Furthermore, mutagenesis identifies K525 in SHD1 as a key residue for Asp recognition. The α -factor uptake and Wsc1p endocytosis assays highlight the essential role of the SHD1 binding pocket in NPFxD-mediated receptor internalization *in vivo*.

Given the overall similarities between endocytic mechanisms in yeast and mammals, combined with the relationship between SHD1 and SH3-like domains, it is proposed that the SH3 domain superfamily may be responsible for a much broader and unrecognized array of cargo trafficking events in metazoan organisms.

Materials and methods

Purification of SHD1

A *Saccharomyces cerevisiae* SLA1 fragment encoding residues 495–560 was cloned into the *Bam*HI/*Not*I site of GST fusion vector pGEX-4T-3 (Amersham). The final expressed product was 68 amino acids in length, including Gly and Ser residues at the N-terminus from the vector. *Escherichia coli* Rosetta DE3 pLysS cells were transformed with pGEX-4T-3 containing SHD1 domain and grown either in LB medium or M9 media supplemented with ¹⁵N-labelled NH₄Cl and ¹³C-labelled glucose. The fusion protein was purified from the soluble fraction using glutathione Sepharose 4B beads (Amersham). The GST fusion was cleaved on the beads using thrombin, releasing soluble SHD1 into the solution. A final FPLC purification step based on size exclusion was used to obtain >99% pure SHD1. Mutations were created by site-directed mutagenesis using the Quickchange system (Stratagene) with a template consisting of SLA1 nucleotides 1207–1986 (aa 402–662) subcloned into *Not*I/*Sal*I sites of pBluescriptKS (pBKS-Sla1-1207–1986). pBKS-

Sla1-1207–1986 plasmids containing the mutations were subsequently used as templates to obtain mutant forms of SHD1 (aa 495–560) by PCR and subcloning into the *Bam*HI/*Sal*I site of GST fusion vector pGEX-4T-3 (Stratagene). All mutations and PCR products were confirmed by sequencing. Mutant forms were expressed as GST fusions, cleaved from GST and purified as described above for the wild-type domain.

Information on peptides

Peptides were purchased at >95% purity from Macromolecular Resources at Colorado State University, USA, Cambridge Biosciences, UK and GenScript Corp., USA, and were used without further purification.

NMR spectroscopy

All NMR experiments were performed at 298 K on Varian 600 MHz INOVA system using a sample containing 0.5 mM ¹⁵N/¹³C-labelled SHD1 in complex with 1.0 mM unlabelled Kex2p peptide YNENPFSDPK in PBS (pH 6.7), 1 mM *d*-DTT, 1 mM NaN₃ in 90% H₂O and 10% D₂O. NMR data processing and analysis were performed using NMRpipe and NMRDraw (Delaglio *et al*, 1995) and SPARKY (Goddard and Kneller, 2004). The ¹H, ¹³C and ¹⁵N assignments were obtained using the standard 3D-heteronuclear NMR experiments (Cavanagh *et al*, 1996). NOE-based interproton distance restraints were obtained from ¹⁵N-edited and ¹⁵N/¹³C-simultaneously edited NOESY HSQC ($\tau_m = 150$ ms) experiments. Intermolecular NOEs were obtained from 2D ¹³C-edited, ¹⁵N/¹³C-filtered NOESY ($\tau_m = 150$ ms) experiments (Zwahlen *et al*, 1997). NOE intensities were classified as strong (0.0–3.0 Å), medium (0.0–4.0 Å) and weak (0.0–5.0 Å). Dihedral restraints were obtained from TALOS (Cornilescu *et al*, 1999) and were used with a range of 2 σ about the mean value. Hydrogen bonding constraints were generated for residues in regular secondary structure elements based on the NOE data and lack of exchange cross peaks with water in the ¹⁵N-edited NOESY spectrum. Each hydrogen bond was represented by two distance constraints: 0.0 Å $\leq d_{H-O} \leq 2.0$ Å and 0.0 Å $\leq d_{N-O} \leq 3.0$ Å.

Structure calculation

Initial structure calculations were carried out using CYANA (Guntert, 2004) to refine NOE assignments, which were then used as an input for the simulated annealing-based structure refinement protocol in CNS as implemented in ARIA1.2 (Brunger *et al*, 1998; Lingg *et al*, 2003). Two hundred structures were calculated and the best 20 used for further analysis. The structures were analyzed using PROCHECK (Laskowski *et al*, 1996).

Model of the complex

HADDOCK (Dominguez *et al*, 2003) was used to dock the NPFSD peptide onto SHD1 with the help of distance restraints based on 17 intermolecular NOEs to Pro and Phe. A mutagenesis-based hydrogen bonding distance restraint of 3 Å between K525 side chain NZ and Asp8 side chain OD1 atoms was used for positioning the Asp residue in the ligand close to K525 in SHD1. For docking using HADDOCK, all surface-accessible residues in SHD1 which exhibited HSQC shifts larger than the mean value (Figure 2A) upon binding to the Kex2p peptide were defined as 'ACTIVE' residues (V501, D502, R503, G505, T506, F507, K508, D510, H522, K525, A526, N527, V529, I531, A532, V533, A534, K537). Surface-accessible neighbouring residues of the ACTIVE residues were defined as 'PASSIVE' (17 in all). For the Kex2p peptide, the NPFSD residues were defined as ACTIVE and the flanking YNE and PIK residues were defined as PASSIVE. Ambiguous interaction restraints were generated using these residues. The interface for the interaction was defined by residues W500–E512 and K520–S539 in SHD1 and E3–P9 in the Kex2p peptide. All the structural restraints used in the calculation of the SHD1 structure were also used during HADDOCK to minimize structural changes to the SHD1 structure during docking. Default parameters were used for the HADDOCK run. A total of 1000 initial docked structures were generated. The best 100 were refined using simulated annealing followed by water refinement, and 20 structures with lowest energies were used for further analysis.

Surface plasmon resonance

All SPR experiments were carried out using a BIAcore 3000 instrument and CM5 research grade sensor chips (BIAcore Inc., Piscataway, NJ) at 25°C. A Kex2p peptide, CTYDSVLTNENPFS Δ -PIKQK (the recognition motif is underlined), an endocytically inactive mutant, CTYDSVLTNENPASPDIKQK, and variants in which the Asp was either changed or spaced at different positions from the NPF core, CTYDSVLTNENPFSAPIKQK, CTYDSVLTNENPFDPIKQK, CTYDSVLTNENPFSGDPIKQK and CTYDSVLTNENPFSGGDPIKQK, were coupled to the sensor chip via the added cysteine at similar levels (~800 RU) according to the manufacturer's instructions (BIAcore Inc., Piscataway, NJ). Wild-type SHD1 and the mutants in 10 mM HEPES, 150 mM NaCl, 3 mM EDTA and 0.005% surfactant P-20, pH 7.0 HBS buffer were passed over the surfaces at different concentrations at a flow rate of 10 μ l/min for 3 min, followed by a 3 min injection of HBS buffer. The surfaces were then regenerated by a 2 min injection of 4 M guanidine hydrochloride. Dissociation constants were calculated using steady-state affinity fitting with BIAevaluation 4.0 software.

Yeast two-hybrid analysis

For yeast two-hybrid analysis, wild-type and mutant SHD1 fragments were obtained from the corresponding pGex4T3 plasmid after BamHI and SalI digestion and inserted into BamHI and SalI sites of pGAD-C1 to fuse SHD1 domains to the Gal4p activation domain. These constructs were tested for interaction with a construct containing residues 298–318 of Ste2 followed by the sequence VLTNANPFS Δ DP repeated three times in tandem and fused to the Gal4 DNA-binding domain (pGBD-C1) as described previously (Howard *et al*, 2002).

References

Altschul SF, Madden TL, Schaffer AA, Zhang J, Zhang Z, Miller W, Lipman DJ (1997) Gapped BLAST and PSI-BLAST: a new generation of protein database search programs. *Nucleic Acids Res* **25**: 3389–3402
Ayscough KR, Stryker J, Pokala N, Sanders M, Crews P, Drubin DG (1997) High rates of actin filament turnover in budding yeast and

GST-fusion protein affinity assay

pGEX-KG-(NPFSD)₃ and pGEX-KG-(NPASD)₃ contained residues 298–318 of Ste2 followed by three tandem repeats of the sequence VLTNANP(F/A)SDP fused to GST. The GST-fusion proteins were expressed in *E. coli*, purified with glutathione-Sepharose, eluted from the beads with reduced glutathione and dialyzed against PBS (12 mM phosphate, 147 mM NaCl, 3 mM KCl, pH 7.35). Purified GST-(NPFSD)₃ and GST-(NPASD)₃ (50 μ g) were immobilized on to 20 μ l of glutathione-Sepharose beads and incubated with 20 μ g of wild-type or mutant SHD1 domains in a total volume of 1 ml of PBS at 4°C for 90 min. Subsequently, beads were isolated and washed thrice with ice-cold PBS containing 0.2% Triton X-100 and then once with PBS without detergent. The proteins were eluted and analyzed by SDS-polyacrylamide gel electrophoresis (SDS-PAGE).

Yeast strains and endocytosis assays

GPY1805 (*MAT α ura3-52 leu2-3,112 his3- Δ 200 trp1- Δ 901 lys2-801 suc2- Δ 9 sst1 Δ ::LYS2 ste2 Δ ::LEU2* (Howard *et al*, 2002)) was used as the *SLA1* wild-type control strain. Mutations were introduced into endogenously expressed Sla1p with a two-step approach. For the first step, SHD1 flanking sequences, nucleotides 1207–1410 and 1706–1986, were amplified by PCR and cloned into *NotI/BamHI* and *EcoRI/SalI* sites of pBluescriptKS, respectively. A PCR fragment containing *URA3* was then subcloned into *BamHI/EcoRI* sites. The resulting construct was cleaved with *NotI/SalI* and the *URA3* fragment was introduced by lithium acetate transformation (Ito *et al*, 1983) into GPY1805 cells to generate GPY4297 in which SHD1 was replaced with *URA3*. Replacement was confirmed by PCR and sequencing. In the second step, *BsgI/BstBI* fragments from pBKS-Sla1-1207–1986 containing single amino-acid mutations were cotransformed with pRS313 (*HIS3*; Sikorski and Hieter, 1989) into pGPY4297. His⁺ colonies were replica-plated onto 5-fluoroorotic acid plates to identify cells in which mutant SHD1 sequences replaced *URA3*. Regeneration of full-length *SLA1* containing single SHD1 mutations was confirmed by PCR and sequencing. For α -factor endocytosis assays, GPY1805 and *SLA1* mutant strains were transformed with a plasmid encoding a modified version of the α -factor receptor Ste2p, pJH121 (pRS314-STE2 Δ 318-NPFSD) (Howard *et al*, 2002). A cross of the SHD1 mutant strains containing pJH108-11KR-NPF plasmid (Howard *et al*, 2002) to GPY3548 (*MAT α ura3-52 leu2-3,112 his3- Δ 200 trp1- Δ 901 lys2-801 suc2- Δ 9 WSC1-GFP::HIS3 sla1 Δ ::URA3*) was used to generate haploid strains carrying both the SHD1 mutations and Wsc1p-GFP. The wild-type strain used for analysis of Wsc1p-GFP internalization was GPY3527 (*MAT α ura3-52 leu2-3,112 his3- Δ 200 trp1- Δ 901 lys2-801 suc2- Δ 9 WSC1-GFP::HIS3*; Piao *et al*, 2007).

Radiolabeled α -factor preparation and endocytosis assays were performed as previously described (Tan *et al*, 1996; Howard *et al*, 2002), and sensitivity to caspofungin (gift from Ainslie Parsons, University of Toronto) was measured as described by Piao *et al* (2007). In the caspofungin assay, GPY2448 (GPY1805 *sla1 Δ ::HIS3*; Howard *et al*, 2002) was used. Fluorescence microscopy was carried out as in Piao *et al* (2007). All images were captured using a \times 100 objective on a Zeiss Axiovert 200M microscope with a Hamamatsu 9100 EM CCD camera.

Acknowledgements

We thank Dr T de Beer for initiating this collaborative study, HWB-NMR and the UCHSC NMR staff for spectrometer time and assistance, and Drs DNM Jones and F Dancea for help with structure calculations. We thank Drs W Wang, R Lehrer and E Lafer for assistance with BIAcore analysis. This work was funded by grants from NIH (CA92181) and Cancer Research UK (C13365) to MO and NIH (GM39040) to GP. PDB ID: 2HBP (ensemble of 20 lowest energy structures and experimental constraints).

roles for actin in establishment and maintenance of cell polarity revealed using the actin inhibitor latrunculin-A. *J Cell Biol* **137**: 399–416
Ayscough KR, Eby JJ, Lila T, Dewar H, Kozminski KG, Drubin DG (1999) Sla1p is a functionally modular component of the yeast cortical actin cytoskeleton required for correct localization of

- both Rho1p-GTPase and Sla2p, a protein with talin homology. *Mol Biol Cell* **10**: 1061–1075
- de Beer T, Hoofnagle AN, Enmon JL, Bowers RC, Yamabhai M, Kay BK, Overduin M (2000) Molecular mechanism of NPF recognition by EH domains. *Nat Struct Biol* **7**: 1018–1022
- Brunger AT, Adams PD, Clore GM, DeLano WL, Gros P, Grosse-Kunstleve RW, Jiang JS, Kuszewski J, Nilges M, Pannu NS, Read RJ, Rice LM, Simonson T, Warren GL (1998) Crystallography & NMR system: a new software suite for macromolecular structure determination. *Acta Crystallogr D* **54**: 905–921
- Cavanagh J, Fairbrother WJ, Palmer III AG, Skelton NJ (1996) *Protein NMR Spectroscopy*. San Diego: Academic Press Inc.
- Cornilescu G, Delaglio F, Bax A (1999) Protein backbone angle restraints from searching a database for chemical shift and sequence homology. *J Biomol NMR* **13**: 289–302
- Delaglio F, Grzesiek S, Vuister GW, Zhu G, Pfeifer J, Bax A (1995) NMRPipe: a multidimensional spectral processing system based on UNIX pipes. *J Biomol NMR* **6**: 277–293
- DeLano WL (2002) *The PYMOL Molecular Graphics System*. San Carlos, CA: DeLano Scientific
- Domínguez C, Boelens R, Bonvin AMJJ (2003) HADDOCK: a protein–protein docking approach based on biochemical or biophysical information. *J Am Chem Soc* **125**: 1731–1737
- Engqvist-Goldstein AE, Drubin DG (2003) Actin assembly and endocytosis: from yeast to mammals. *Ann Rev Cell Dev Biol* **19**: 287–332
- Goddard TD, Kneller DG (2004) *SPARKY 3*. San Francisco: University of California
- Gourlay CW, Dewar H, Warren DT, Costa R, Satish N, Ayscough KR (2003) An interaction between Sla1p and Sla2p plays a role in regulating actin dynamics and endocytosis in budding yeast. *J Cell Sci* **116**: 2551–2564
- Güntert P (2004) Automated NMR structure calculation with CYANA. *Methods Mol Biol* **278**: 353–378
- Hicke L, Dunn R (2003) Regulation of membrane protein transport by ubiquitin and ubiquitin-binding proteins. *Annu Rev Cell Dev Biol* **19**: 141–172
- Holm L, Sander C (1993) Protein structure comparison by alignment of distance matrices. *J Mol Biol* **233**: 123–138
- Holtzman DA, Yang S, Drubin DG (1993) Synthetic-lethal interactions identify two novel genes, *SLA1P* and *SLA2*, that control membrane cytoskeleton assembly in *Saccharomyces cerevisiae*. *J Cell Biol* **122**: 635–644
- Howard JP, Hutton JL, Olson JM, Payne GS (2002) Sla1p serves as the targeting signal recognition factor for NPF(1,2)D-mediated endocytosis. *J Cell Biol* **157**: 315–326
- Ito H, Fukuda Y, Murata K, Kimura A (1983) Transformation of intact yeast cells treated with alkali cations. *J Bacteriol* **153**: 163–168
- Kaksonen M, Toret CP, Drubin DG (2005) A modular design for the clathrin- and actin-mediated endocytosis machinery. *Cell* **123**: 305–320
- Kaksonen M, Toret CP, Drubin DG (2006) Harnessing actin dynamics for clathrin-mediated endocytosis. *Nat Rev Mol Cell Biol* **7**: 404–414
- Koradi R, Billeter M, Wuthrich K (1996) MOLMOL: a program for display and analysis of macromolecular structures. *J Mol Graph* **14**: 51–55
- Laskowski RA, Rullmann JAC, MacArthur MW, Kaptein R, Thornton JM (1996) AQUA and PROCHECK-NMR: programs for checking the quality of protein structures solved by NMR. *J Biomol NMR* **8**: 477–486
- Linge JP, Habek M, Rieping W, Nilges M (2003) ARIA: automated NOE assignment and NMR structure calculation. *Bioinformatics* **19**: 315–316
- Massenet C, Chenavas S, Cohen-Addad C, Dagher MC, Brandolin G, Pebay-Peyroula E, Fieschi F (2005) Effects of p47phox C terminus phosphorylations on binding interactions with p40phox and p67phox. Structural and functional comparison of p40phox and p67phox SH3 domains. *J Biol Chem* **280**: 13752–13761
- Owen DJ, Collins BM, Evans PR (2004) Adaptors for clathrin coats: structure and function. *Annu Rev Cell Dev Biol* **20**: 153–191
- Perrais D, Merrifield CJ (2005) Dynamics of endocytic vesicle creation. *Dev Cell* **9**: 581–592
- Piao HL, Machado IM, Payne GS (2007) NPFxD-mediated endocytosis is required for polarity and function of a yeast cell wall stress sensor. *Mol Biol Cell* **18**: 57–65
- Schumacher MA, Pearson RF, Moller T, Valensin-Hansen P, Brennan RG (2002) Structures of the pleiotropic translational regulator Hfq and an Hfq-RNA complex: a bacterial Sm-like protein. *EMBO J* **21**: 3546–3556
- Sikorski RS, Hieter P (1989) A system of shuttle vectors and yeast host strains designed for efficient manipulation of DNA in *Saccharomyces cerevisiae*. *Genetics* **122**: 19–27
- Stamenova SD, Dunn R, Adler AS, Hicke L (2004) The Rsp5 ubiquitin ligase binds to and ubiquitinates members of the yeast CIN85-endophilin complex, Sla1-Rvs167. *J Biol Chem* **279**: 16017–16025
- Stolt PC, Jeon H, Song HK, Herz J, Eck MJ, Blacklow SC (2003) Origins of peptide selectivity and phosphoinositide binding revealed by structures of disabled-1 PTB domain complexes. *Structure* **11**: 569–579
- Subramaniam S (1998) The Biology Workbench—a seamless database and analysis environment for the biologist. *Protein Struct Funct Genet* **32**: 1–2
- Tan PK, Howard JP, Payne GS (1996) The sequence NPFxD defines a new class of endocytosis signal in *Saccharomyces cerevisiae*. *J Cell Biol* **135**: 1789–1800
- Thompson JD, Higgins DG, Gibson TJ (1994) CLUSTAL W: improving the sensitivity of progressive multiple sequence alignment through sequence weighting, position-specific gap penalties and weight matrix choice. *Nucleic Acids Res* **22**: 4673–4680
- Traub LM (2005) Common principles in clathrin-mediated sorting at the Golgi and the plasma membrane. *Biochim Biophys Acta* **1744**: 415–437
- Zeng G, Yu X, Cai M (2001) Regulation of yeast actin cytoskeleton-regulatory complex Pan1p/Sla1p/End3p by serine/threonine kinase Prk1p. *Mol Biol Cell* **12**: 3759–3772
- Zwahlen C, Legault P, Vincent SJF, Greenblatt J, Konrat R, Kay LE (1997) Measurement of intermolecular NOE's by multinuclear NMR spectroscopy: application to a bacteriophage λ N-peptide/boxB RNA complex. *J Am Chem Soc* **119**: 6711–6721